AIChE WILEY InterScience DISCOVER SOMETHING GREAT

Drying of Two-Phase Media: Simulation with Liquid Pressure as Driven Force

Frédéric Couture, Stéphane Laurent, and Michel A. Roques
LaTEP–E.N.S.G.T.I., Rue Jules Ferry, BP 7511, 64075 Pau Cedex, France

DOI 10.1002/aic.11213
Published online June 1, 2007 in Wiley InterScience (www.interscience.wiley.com).

In previous works, a model based on volume averaging theory to describe heat and mass transports in two-phase media has been proposed. The main novelty was to consider both mass and volume conservation of the solid phase in order to avoid the introduction of an arbitrarily law binding the pressure to the volume fraction of the liquid phase. Indeed, this law leads to an equivalent transport coefficient that must be identified numerically by matching experimental and predicted data in such a way that process and internal model become unjustly dependant. Here, the mathematical description is solved. The forecasting of damages and cracks during drying of fully saturated media incites us to simulate transport phenomena which occur in gel (gelatin) during this process. Although the one-dimensional configuration which is considered leads us to reduce the elastic behavior to an ideal shrinkage, the numerical results and the qualitative comparison to experimental measures provide some confidence in the proposed model. © 2007 American Institute of Chemical Engineers *AIChE J,* 53: 1703–1717, 2007
Keywords: fluid mechanics and transport phenomena, modeling, volume averaging, deformable medium, gel

Introduction

Transport phenomena that occur in highly deformable media during solid liquid separation process have been discussed by numerous authors.[1,2] Most of the materials under investigation are considered reasonably as two-phase systems: a solid phase and a liquid phase. Whatever the modeling approach may be (averaging theory, irreversible thermodynamics, intuitive equivalence to a continuous medium), a similar mathematical description which consists of heat, mass, and momentum conservation laws is needed. Deformations are always taken into account by using the sum of the momentum conservation of each phase. Under the commonly used assumption that the motion of each phase is quasi-steady, this relation that we will call *total momentum conservation* represents a mechanical equilibrium of the global diphasic medium under a load depending on the process; for instance, it is the shrinkage due to solvent removal during drying or the pressure applied during filtration and expression. However, one can distinguish in literature two kinds of treatment of the total momentum conservation depending on the stress strain relation that is introduced. Some authors[3–5] choose to sum a solid relation and a liquid one. This implies neglect of the viscosity effects in the liquid rheological law, but without any consistency, keeping them in the liquid flux expression as Darcy's law. Moreover, the measurement of the stress strain relation for the solid phase seems difficult. Other authors such as us prefer to consider the rheological behavior of the total two phase system by introducing a unique law experimentally determined on the humid medium. The main inconvenience is then how to treat the unknown liquid pressure in so far as it does not appear in the total momentum conservation. Most of the authors circumvent this difficulty by introducing arbitrarily a phenomenological law, which supposes that the pressure depends on the liquid volume fraction.[6–11] This law constitutes an important limitation to the analysis of transport mechanisms. From a physical point of view, the driving force is undoubtedly without any

Correspondence concerning this article should be addressed to S. Laurent at stephane.laurent@univ-pau.fr.

© 2007 American Institute of Chemical Engineers

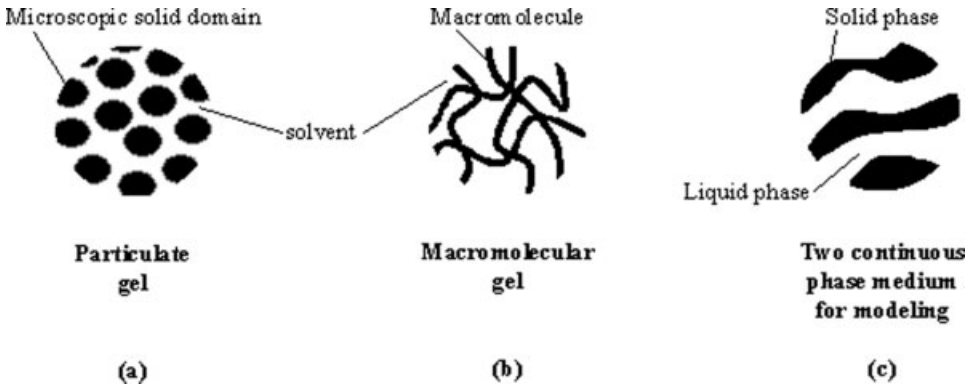

Figure 1. Schemes of the microstructure of gels (a), (b) and identification to two continuous phase medium for the modeling (c).

foundations. From a practical point of view, an equivalent transport coefficient must be identified numerically by matching experimental and predicted data in such a way that further validation is rendered without interest. Moreover, whatever the process examined, our feeble knowledge in the mathematical description of the boundary conditions leads to an internal transport coefficient intimately linked to the process. This dependence contrasts obviously with the aim of proposing a model valid for a wide range of solid liquid separation processes.

The main novelty of the model proposed in a previous work of ours[12] is that such a coefficient is not introduced although at the same time a global stress strain relation is used. A continuum approach based on volume averaging theory[13] was adopted. Conservation equations are first written for each phase. The macroscopic partial differential equations are derived by integrating over a representative volume of these microscopic conservation laws. At this stage, the question of how to treat rigorously the area integral in the liquid and solid momentum balances still remains unanswered. The solid momentum conservation is replaced by its sum with the liquid momentum conservation to give the previously discussed total momentum conservation. By introducing, at the phase scale, the rheological behavior of a classic fluid for the liquid phase in the liquid momentum conservation and by integrating the obtained equation, Darcy's law is established.[13,14] This law, which links the average liquid velocity to the pressure gradient, can be used to replace the liquid momentum conservation. The assumption that the volume of each phase is conserved (incompressibility) gives the two supplementary equations that are necessary to close the macroscopic description. In the literature, only volume conservation of the solid phase is kept, solid mass conservation being ignored under the fallacious pretext that the two equations are redundant. Besides, one can note the incoherence present in considering mass and volume conservation as similar for the solid phase and at the same time, in using both volume and mass conservation for the liquid phase. As a result, there is one equation missing. In order to fill in this loss, the arbitrary link between liquid pressure and liquid volume fraction leading to the equivalent transport coefficient previously mentioned is introduced. Here, both volume and mass conservation equations are kept for the solid phase in such a way that the introduction of an nonphysical law becomes unnecessary.

After being reviewed, the model is solved in order to simulate transport phenomena which occur during low or middle temperature convective drying of gelatin. Both the process and the material have been chosen for the following two main reasons. Gelatin is a gel that has been well identified in the past for temperatures in the range of 0–100°C. All the transport coefficients needed for the simulation are available in literature.[15–18] It is assumed here to consist of a solid phase and a water phase. For convective drying, closure of the system by boundary conditions can be obtained correctly by using the boundary layer theory and the classical Lewis analogy. Only one-dimensional configuration is considered. It implies reduction of the elastic behavior to an ideal shrinkage. However, the numerical results and the qualitative comparison to experimental data provide some confidence in the proposed model.

Modeling

A necessary preliminary to the mathematical formulation is to define precisely the range of the products which are concerned. As previously mentioned, media under investigation are industrial products known as gels. Two kinds of gel can be distinguished.

- *Particulate gels* could be described as stacking and assembling of microscopic domains (1–100 μm). A schematic representation is proposed in Figure 1a. This subgroup contains paints, silica, alumina, clays, and many other oxides.
- *Macromolecular gels* group contains agarose, gelatine, starch, polyacrylates, glues, and reticulating varnishes. As illustrated in Figure 1b, they consist of long interwoven chains of macromolecules. The interlocking can be fixed covalent bonding such as in polyacrylamide or mobile sliding such as in gelatine.

The complexity and our limited knowledge of the above-described microstructures contrast with our aim of proposing a modeling valid for a wide range of material and imply use of a homogenization method that permits erasing of microscopic heterogeneity. We chose the volume averaging.[13,19–22] However, applying the theory imposes the following assump-

tion: the sophisticated microstructure of the gel is "simplified" to two continuous immiscible phases, a liquid and a solid one (Figure 1c). Indeed, the macroscopic description (or local scale description) is provided by integrating over a representative volume the microscopic (or phase scale) conservation laws. These laws and the associated boundary conditions linking the two phases are written for each phase on the basis of the continuum physics. Given the previous definition of particulate and macromolecular gels, to consider a two-phase system could be the most important limitation of our entire analysis. The solid microscopic domains or chains of macromolecules form perhaps a discontinuous solid phase. Here, we assume the assimilation to a two-phase system for modeling purpose.

Although the mathematical developments necessary to pass from the scale phase description to the local one are not presented here, both the two descriptions are presented in order to emphasize the physical origin of the relations used. All the notations are given in the nomenclature.

Phase scale equations

The mass, momentum, and heat transports are initially described for each phase by classical balance equations as well as the boundary conditions in the phase scale, where the subscripts L and S mean liquid and solid phases respectively.

Liquid Phase. The mass conservation for the liquid phase is directly represented by the continuity equation:

$$\frac{\partial \rho_L}{\partial t} + \nabla \cdot (\rho_L \mathbf{v}_L) = 0 \tag{1}$$

If one assumes a porous structure for the material under investigation, the characteristic pore diameter $2r$ is very small. The characteristic time for flow in porous media ($4r^2/v_L$ with v_L the kinematic viscosity[21]) is of the order of 10^{-2}, 10^{-3}, or less. Characteristic times for the liquid–solid separation processes examined are generally of the order of minutes. Thus, the process is treated reasonably as quasi-steady. The small size of the pore allows also neglecting the gravity. As in literature, we assume that the convective inertial effects are negligible for most problems of interest.[13,21] Thus, the liquid momentum conservation equation for a mono-component phase is

$$\nabla \cdot \underline{\underline{\boldsymbol{\sigma}}}_L = 0. \tag{2}$$

The energy conservation equation is written

$$\frac{\partial}{\partial t}(\rho_L h_L) + \nabla \cdot (\rho_L \mathbf{v}_L h_L) = \nabla \cdot (\lambda_L \nabla T_L). \tag{3}$$

Here it is considered that there are no external sources. The viscous dissipation and the work pressure are neglected. The validity of these two last assumptions is discussed elsewhere.[21,22]

At this stage, for a fluid phase, mass conservation, momentum conservation, and energy conservation constitute five scalar equations, which are not enough to describe phenomena. One more equation is necessary to obtain the six scalar unknowns: density, the three components of the velocity, temperature and the liquid pressure, which comes from the rheological behavior of the newtonian liquid. The additional equation can be provided by considering the flow of the liquid phase as incompressible

$$\rho_L = \text{cst.} \tag{4}$$

Let us underline that this last equation is not a simplification of the mass conservation (1) but a new independent relation that expresses the volume conservation. Indeed, relation (4) in relation (1) leads to the typical equation obtained when the volume of a domain remains constant during motion:

$$\nabla \cdot \mathbf{v}_L = 0. \tag{5}$$

Solid Phase. Under the same assumptions, a description similar to the liquid phase one is obtained for the solid phase:

$$\frac{\partial \rho_S}{\partial t} + \nabla \cdot (\rho_S \mathbf{v}_S) = 0, \tag{6}$$

$$\nabla \cdot \underline{\underline{\boldsymbol{\sigma}}}_S = 0, \tag{7}$$

$$\frac{\partial}{\partial t}(\rho_S h_S) + \nabla \cdot (\rho_S \mathbf{v}_S h_S) = \nabla \cdot (\lambda_S \nabla T_S). \tag{8}$$

It is also reasonable to consider the movement of the solid phase as incompressible:

$$\rho_S = \text{cst.} \tag{9}$$

Contrary to (4) for the liquid phase, this last equation is not necessary to provide a complete modeling of the solid phase. Indeed, the five scalar equations consisting of mass, momentum, and energy balances lead to the five scalar unknowns: density, the three components of the velocity, and temperature. Contrary to liquid or gas, pressure does not appear in stress–strain relation of the solid phase. To sum up, Eq. 9 is an extra equation for the solid phase. Rigorously, it means that one equation should be removed. In literature[6–11] the mass conservation equation for the solid phase is commonly chosen. However, in this work all equations are kept at this moment because this extra equation will be helpful to not use a phenomenological law later. In fact, the average of this extra equation, Eq. 9, will replace the arbitrary link between averaged liquid pressure and liquid volume fraction introduced in literature.

Boundary Conditions. The boundary conditions at the liquid–solid interface close the phase scale description:

$$\rho_L(\mathbf{v}_L - \mathbf{w}) \cdot \mathbf{n}_{LS} = 0, \tag{10}$$

$$\rho_S(\mathbf{v}_S - \mathbf{w}) \cdot \mathbf{n}_{SL} = 0, \tag{11}$$

$$\underline{\underline{\boldsymbol{\sigma}}}_L \cdot \mathbf{n}_{LS} + \underline{\underline{\boldsymbol{\sigma}}}_S \cdot \mathbf{n}_{SL} = 0, \tag{12}$$

$$T_S = T_L = T, \tag{13}$$

$$(\lambda_L \nabla T_L) \cdot \mathbf{n}_{LS} + (\lambda_S \nabla T_S) \cdot \mathbf{n}_{SL} = 0, \tag{14}$$

where $\mathbf{n}_{LS}$ and $\mathbf{n}_{SL}$ are unit vectors normal to the common surface of the solid and liquid phases.

At this point, transport phenomena are described rigorously. However, the solution of these equations requires knowledge of the microscopic geometry and a very important computational time. The volume averaging allows overcoming of this difficulty and leads to the local scale description constituted of the averaged previous equations.

Local scale equations

The development, details, and hypothesis to obtain the local scale equations can be found notably in Refs. 13, 21, and 23 and are reviewed in Ref. 14. In this work, only the summary of the local scale equations obtained by the method of the volume averaging is presented. By integrating over the representative volume V the phase scale conservation laws, the value of any physical quantity Ψ associated to the phase α $(= \mathrm{L}, \mathrm{S})$ at a point in space is given by its average value on the averaging volume V centered on this point. One can distinguish the phase average $\bar{\Psi}$ and the intrinsic phase average $\bar{\Psi}^{\alpha}$defined respectively as

$$\bar{\Psi} = \frac{1}{V}\int_{V_\alpha} \Psi_\alpha dV,$$

$$\bar{\Psi}^{\alpha} = \frac{1}{V_\alpha}\int_{V_\alpha} \Psi_\alpha dV,$$

where V_α is the volume of the phase α within the averaging volume V. The deviation of Ψ, difference between the phase scale value and the intrinsic phase average, can appear when a product is averaged:

$$\tilde{\Psi} = \Psi - \bar{\Psi}^{\alpha}.$$

First of all, the two parameters which are induced by the change in scale have to be introduced. The volume fractions for the two phases are linked as the medium remains fully saturated during the overall process,

$$\varepsilon_\mathrm{S} + \varepsilon_\mathrm{L} = 1, \tag{15}$$

with

$$\varepsilon_\alpha = V_\alpha/V, \quad \alpha = \mathrm{L}, \mathrm{S}.$$

This means the theory implies one unknown that is not an averaged value of one unknown defined at the phase scale. It is why the volume conservation (9) of the solid phase, which was an additional equation at the phase scale, must be kept and averaged at the same time when the mass conservation (6) is averaged. Thus, number of equations and number of unknowns will be the same without introducing supplementary nonphysical laws.

Averaged equations for the mass, momentum, and heat transports obtained from the liquid phase Eqs. 1–4 are

$$\frac{\partial \bar{\rho}_\mathrm{L}}{\partial t} + \nabla \cdot \left(\bar{\rho}_\mathrm{L}\bar{\mathbf{v}}_\mathrm{L}^{\mathrm{L}}\right) = 0, \tag{16}$$

$$\nabla \cdot \bar{\underline{\boldsymbol{\sigma}}}_\mathrm{L} + \frac{1}{V}\int_{A_\mathrm{SL}} \underline{\boldsymbol{\sigma}}_\mathrm{L} \cdot \mathbf{n}_\mathrm{LS} dA = 0, \tag{17}$$

$$\begin{aligned}\frac{\partial}{\partial t}\left(\bar{\rho}_\mathrm{L}\bar{h}_\mathrm{L}^{\mathrm{L}}\right) + \nabla \cdot \left(\bar{\rho}_\mathrm{L}\bar{h}_\mathrm{L}^{\mathrm{L}}\bar{\mathbf{v}}_\mathrm{L}^{\mathrm{L}}\right) \\ = \nabla \cdot \left[\lambda_\mathrm{L}\left(\nabla \bar{T}_\mathrm{L} + \frac{1}{V}\int_{A_\mathrm{SL}} T_\mathrm{L}\mathbf{n}_\mathrm{LS} dA\right) - \bar{\rho}_\mathrm{L}^{\mathrm{L}}\overline{\tilde{h}_\mathrm{L}\tilde{\mathbf{v}}_\mathrm{L}}\right] \\ + \frac{1}{V}\int_{A_\mathrm{SL}} \lambda_\mathrm{L}\nabla T_\mathrm{L} \cdot \mathbf{n}_\mathrm{LS} dA,\end{aligned} \tag{18}$$

$$\bar{\rho}_\mathrm{L}^{\mathrm{L}} = \mathrm{cst}. \tag{19}$$

In the same way the Eqs. for the solid phase 6–9 produce

$$\frac{\partial \bar{\rho}_\mathrm{S}}{\partial t} + \nabla \cdot \left(\bar{\rho}_\mathrm{S}\bar{\mathbf{v}}_\mathrm{S}^{\mathrm{S}}\right) = 0, \tag{20}$$

$$\nabla \cdot \bar{\underline{\boldsymbol{\sigma}}}_\mathrm{S} + \frac{1}{V}\int_{A_\mathrm{SL}} \underline{\boldsymbol{\sigma}}_\mathrm{S} \cdot \mathbf{n}_\mathrm{SL} dA = 0, \tag{21}$$

$$\begin{aligned}\frac{\partial}{\partial t}\left(\bar{\rho}_\mathrm{S}\bar{h}_\mathrm{S}^{\mathrm{S}}\right) + \nabla \cdot \left(\bar{\rho}_\mathrm{S}\bar{h}_\mathrm{S}^{\mathrm{S}}\bar{\mathbf{v}}_\mathrm{S}^{\mathrm{S}}\right) \\ = \nabla \cdot \left[\lambda_\mathrm{S}\left(\nabla \bar{T}_\mathrm{S} + \frac{1}{V}\int_{A_\mathrm{SL}} T_\mathrm{S}\mathbf{n}_\mathrm{SL} dA\right) - \bar{\rho}_\mathrm{S}^{\mathrm{S}}\overline{\tilde{h}_\mathrm{S}\tilde{\mathbf{v}}_\mathrm{S}}\right] \\ + \frac{1}{V}\int_{A_\mathrm{SL}} \lambda_\mathrm{S}\nabla T_\mathrm{S} \cdot \mathbf{n}_\mathrm{SL} dA,\end{aligned} \tag{22}$$

$$\bar{\rho}_\mathrm{S}^{\mathrm{S}} = \mathrm{cst}. \tag{23}$$

The previous momentum and energy conservation equations contain area integrals and deviations which can not be computed. The following last part is devoted to the treatment of these terms.

Concerning the energy conservations (18) and (22), the hypothesis of the thermodynamical equilibrium[24] is assumed commonly:

$$\bar{T}_\mathrm{L}^{\mathrm{L}} = \bar{T}_\mathrm{S}^{\mathrm{S}} = \bar{T}. \tag{24}$$

With this assumption and the boundary condition (14), the sum of Eqs. 18 and 22 leads to

$$\begin{aligned}\frac{\partial}{\partial t}\left(\bar{\rho}_\mathrm{S}\bar{h}_\mathrm{S}^{\mathrm{S}} + \bar{\rho}_\mathrm{L}\bar{h}_\mathrm{L}^{\mathrm{L}}\right) + \nabla \cdot \left(\bar{\rho}_\mathrm{S}\bar{h}_\mathrm{S}^{\mathrm{S}}\bar{\mathbf{v}}_\mathrm{S}^{\mathrm{S}} + \bar{\rho}_\mathrm{L}\bar{h}_\mathrm{L}^{\mathrm{L}}\bar{\mathbf{v}}_\mathrm{L}^{\mathrm{L}}\right) \\ = \nabla \cdot \left(\underline{\bar{\lambda}}_{\mathrm{eff}} \cdot \nabla \bar{T}\right),\end{aligned} \tag{25}$$

with

$$\bar{h}_\mathrm{L}^{\mathrm{L}}(\bar{T}, \varepsilon_\mathrm{L}) = Cp_\mathrm{L}(\bar{T} - T_{\mathrm{ref}}) - \overline{\Delta H}_\mathrm{D}^{\mathrm{L}}(\bar{T}, \varepsilon_\mathrm{L}), \tag{26}$$

$$\bar{h}_\mathrm{S}^{\mathrm{S}}(\bar{T}) = Cp_\mathrm{S}(\bar{T} - T_{\mathrm{ref}}), \tag{27}$$

and by assuming

$$\underline{\underline{\boldsymbol{\lambda}}}_{\text{eff}} \cdot \nabla \bar{T} = \lambda_S \nabla \bar{T}_S + \lambda_L \nabla \bar{T}_L + \frac{\lambda_S - \lambda_L}{V} \int_{A_{SL}} T \mathbf{n}_{SL} dA - \bar{\rho}_S^S \overline{\tilde{h}_S \tilde{\mathbf{v}}_S} - \bar{\rho}_L^L \overline{\tilde{h}_L \tilde{\mathbf{v}}_L}. \quad (28)$$

The conductivity tensor $\underline{\underline{\boldsymbol{\lambda}}}_{\text{eff}}$ is given by experiments and $\overline{\Delta H}_D^L$ designates the desorption enthalpy which has to be added to the latent heat of vaporisation in order to eliminate the bound liquid. Equation 26 expresses both the enthalpy of the bound and free liquid phase from the state of reference defined as the free liquid phase at T_{ref}. If the liquid phase is free, the desorption enthalpy $\overline{\Delta H}_D^L$ is equal to zero.

The problem of area integrals in the energy conservation equations is then solved by replacing Eqs. 18 and 22 by Eqs. 24 and 25.

In the same way, the sum of the momentum conservation Eqs. 17 and 21 can be used to remove partially the difficulty induced by the microscopic terms. The result replaces the solid momentum conservation. Thus, by adding and taking into account the boundary condition 12, we obtain for the total momentum conservation

$$\nabla \cdot \bar{\underline{\underline{\boldsymbol{\sigma}}}} = 0, \quad (29)$$

with

$$\bar{\underline{\underline{\boldsymbol{\sigma}}}} = \bar{\underline{\underline{\boldsymbol{\sigma}}}}_L + \bar{\underline{\underline{\boldsymbol{\sigma}}}}_S. \quad (30)$$

Under the quasi-steady hypothesis, the Eq. 29 represents successive mechanical equilibrium states of the deformable medium under the load induced by the shrinkage due to liquid removal.

At this stage, only the area integral in the liquid momentum balance 17 remains. To circumvent this main difficulty, the first classical step is to replace the Eq. 17 by the Darcy's law derived rigorously from the integration of the liquid momentum conservation 2 in which the rheological behavior of the newtonian liquid phase has been introduced,[13,14,21]

$$\bar{\mathbf{v}}_L^L - \bar{\mathbf{v}}_S^S = -\frac{1}{\varepsilon_L \mu_L} \underline{\underline{\mathbf{K}}} \cdot \nabla \bar{P}_L^L. \quad (31)$$

Two kinds of treatment of the total momentum conservation (29) depending on the stress strain relation which is introduced can be distinguished. A first technique consists in adding an averaged liquid relation and a solid one.[3–5] The rheological behavior of the liquid phase is justly considered as newtonian and the average of the viscous stress tensor is always neglected. The solid stress strain relation has to be determined experimentally.

$$\bar{\underline{\underline{\boldsymbol{\sigma}}}} = -\varepsilon_L \bar{P}_L^L \underline{\underline{\mathbf{I}}} + \bar{\underline{\underline{\boldsymbol{\sigma}}}}_S. \quad (32)$$

The main advantage of this approach is that the introduction of Eq. 32 in the total momentum conservation 29 and an adequate combination of the other conservation equations allow obtaining of the liquid volume fraction without the calculation of the liquid pressure. However, to neglect in the liquid rheological law the viscosity effects, but at the same time, to keep them in the liquid flux expression as Darcy's law (Eq. 31) constitutes a contradiction, which encourages us—as it has other authors[6–11]—to adopt a second method. The rheological behavior of the total two phase system is considered by introducing a unique law experimentally determined in order to express the total stress tensor $\bar{\underline{\underline{\boldsymbol{\sigma}}}}$ in term of strain.

For instance, the dependent moisture stress–strain relation for an elastic behavior can be expressed as follows:

$$\bar{\underline{\underline{\boldsymbol{\sigma}}}} = \lambda(\varepsilon_L) \text{tr} \underline{\underline{\boldsymbol{\varepsilon}}}^* + 2\mu(\varepsilon_L) \underline{\underline{\boldsymbol{\varepsilon}}}^*. \quad (33)$$

In the above expression, $\underline{\underline{\boldsymbol{\varepsilon}}}^*$is the elastic strain tensor and is not the total strain tensor $\underline{\underline{\boldsymbol{\varepsilon}}}$ associated to the total shrinkage. Indeed, most of the total strain is induced by the volume change due to the liquid migration. By noting $\underline{\underline{\boldsymbol{\varepsilon}}}^v$ the tensor which characterizes this volumetric strain, it ensues:

$$\underline{\underline{\boldsymbol{\varepsilon}}} = \underline{\underline{\boldsymbol{\varepsilon}}}^* + \underline{\underline{\boldsymbol{\varepsilon}}}^v. \quad (34)$$

In term of displacements, this tensor is given by:

$$\underline{\underline{\boldsymbol{\varepsilon}}} = \frac{1}{2}\left[(\nabla \otimes \bar{\mathbf{u}}) + (\nabla \otimes \bar{\mathbf{u}})^T\right]. \quad (35)$$

As it is indicated by Eq. 34, the volumetric shrinkage would be the real shrinkage value if the material did not build up stresses during the process (case of ideal shrinkage). The supplementary elastic stress influences the shrinkage by reducing it to smaller values due to internal forces acting against the free deformation. The rheological functions known as Lamé's parameters depend on moisture and as previously mentioned, they have to be measured by experiments carried out on the humid medium.

Undoubtedly more accurate on a technical point of view, use of the total stress tensor induces a main inconvenience: how to treat the unknown liquid pressure in so far as it does not appear in the total momentum conservation. Most of the authors circumvent this difficulty by postulating arbitrarily a phenomenological law which supposes that the liquid pressure is linked to the liquid volume fraction[6–11]:

$$\bar{P}_L^L = f(\varepsilon_L). \quad (36)$$

This phenomenological law in the Darcy's law (Eq. 31) leads to

$$\bar{\mathbf{v}}_L^L - \bar{\mathbf{v}}_S^S = -\underline{\underline{\mathbf{D}}} \cdot \nabla \varepsilon_L, \quad (37)$$

where an equivalent transport tensor $\underline{\underline{\mathbf{D}}}$ appears:

$$\underline{\underline{\mathbf{D}}} = \frac{\underline{\underline{\mathbf{K}}}}{\mu_L \varepsilon_L} \frac{\partial \bar{P}_L^L}{\partial \varepsilon_L}. \quad (38)$$

Two situations have to be distinguished. If the solid mass conservation Eq. 6 has been removed at the phase scale under the assumption of the incompressibility Eq. 9, the above relation 36 is an additional equation which enables the closure of the problem by ensuring the equality between the number of unknowns and the number of equations (let us remember that the change in scale implies one more unknown, see the beginning of the section entitled "local scale equations"). If both solid mass conservation Eq. 6 and incompressibility relation 9 have been kept and averaged to

give Eqs. 20 and 23 respectively, the above relation 36 is an additional equation that avoids the numerical resolution of one of the averaged conservation laws. Usually, the mass conservation of the solid phase Eq. 20 is eliminated. Whatever the case, the law 36 prevents a rigorous analysis of transport phenomena. Indeed, this relation being without physical foundations, the mathematical relation in order to express the liquid pressure in term of liquid volume fraction is not available. Contrary to the permeability tensor $\underline{\underline{\mathbf{K}}}$, $\underline{\underline{\mathbf{D}}}$ cannot be determined experimentally. It has to be identified numerically by matching experimental and simulated data. Whatever the experimental set-up, the poor knowledge in the mathematical description of the boundary conditions leads to an internal transport coefficient intimately linked to the apparatus. This dependence is not admissible when the aim is to propose a model in order to describe internal transports valid for any solid liquid separation process. Besides one can underline that experimental validation becomes irrelevant.

Here, we avoid introducing Eq. 36 by taking inspiration from previous studies dealing with multicomponent mass transport during dehydration impregnation soaking.[25,26] Rather than being removed under the assumption of the incompressibility of the solid phase 23 or under the introduction of the nonphysical law 36, the solid mass conservation 20 enables the unknown liquid pressure $\bar{P}_{\mathrm{L}}^{\mathrm{L}}$ to be computed.

By introducing the volume fraction of the solid phase, the Eq. 20 becomes

$$\frac{\partial}{\partial t}\left(\varepsilon_{\mathrm{S}}\bar{\rho}_{\mathrm{S}}^{\mathrm{S}}\right)+\nabla\cdot\left(\bar{\rho}_{\mathrm{S}}^{\mathrm{S}}\bar{\mathbf{v}}_{\mathrm{S}}\right)=0. \tag{39}$$

Taking into account the incompressibility 23, it ensues

$$\frac{\partial\varepsilon_{\mathrm{S}}}{\partial t}+\nabla\cdot\bar{\mathbf{v}}_{\mathrm{S}}=0. \tag{40}$$

The same procedure is done for the Eq. 16 and the result is added to Eq. 40

$$\frac{\partial}{\partial t}\left(\varepsilon_{\mathrm{L}}+\varepsilon_{\mathrm{S}}\right)+\nabla\cdot\left(\bar{\mathbf{v}}_{\mathrm{L}}+\bar{\mathbf{v}}_{\mathrm{S}}\right)=0. \tag{41}$$

Applying the Eq. 15, it results

$$\nabla\cdot\left(\bar{\mathbf{v}}_{\mathrm{L}}+\bar{\mathbf{v}}_{\mathrm{S}}\right)=0. \tag{42}$$

Introducing the Darcy's law (Eq. 31), it gives finally

$$\nabla\cdot\left(\bar{\mathbf{v}}_{\mathrm{S}}^{\mathrm{S}}-\frac{1}{\mu_{\mathrm{L}}}\underline{\underline{\mathbf{K}}}\cdot\nabla\bar{P}_{\mathrm{L}}^{\mathrm{L}}\right)=0. \tag{43}$$

The intrinsic average pressure of the liquid phase is provided by the numerical resolution of Eq. 43, the solid velocity resulting from the momentum conservation of the homogenized two-phase medium 29.

To sum up, the model consists of the following averaged equations: the mass conservation equations for each phases 16 and 20, the volume conservation Eqs. 19 and 23 known as incompressibility relations, the momentum conservation Eqs. 29 and 31 which is the Darcy's law, the energy conservation Eqs. 24 and 25 and finally the diphasic state Eq. 15. Here, liquid pressure is an unknown which has to be calculated as liquid volume fraction, solid velocity and temperature.

A first step in the numerical resolution of this model has been undertaken in order to simulate one-dimensional convective drying of gelatin.

Application to One-Dimensional Convective Drying

In this part, the previous model is applied to convective drying. This process, widely described in literature, enables use of the entire model contrary to compression, for instance, which eliminates the heat transport. Moreover, closure of the system by boundary conditions is acceptable by using the boundary layer theory and the classical heat and mass transfer analogy in order to express fluxes. The two-phase medium hypothesis imposes the choice of a highly deformable product like a gel for example. Indeed, the moisture departure is exactly compensated by the solid shrinkage, which prevents the appearance of free spaces for the vapor phase. In this work, the simulations are performed on an elastic gelatin gel. This choice is justified by the existence of a great number of accessible data concerning this material.[15–18]

First, the classical phenomenology of convective drying is reviewed. Then, the initial and boundary conditions are presented as well as the medium properties. To finish, the results of two simulations are analyzed and compared to experiment.

Classical phenomenology of convective drying

The product is exposed to an air flow for which the temperature T_{∞}, the relative humidity $\mathrm{RH}_{\infty}$and the velocity $\mathbf{v}_{\infty}$ are constant. Drying is performed at the atmospheric pressure and with a temperature T_{∞} lower than 100°C. In order to apply the model, a porous structure is supposed for the gel. The moisture is then present under two different forms.

- Free water: The water is not bounded to the solid. The water activity a_{w} is equal to 1 and consequently physical properties of free water are the same that pure liquid water ones. The required energy for evaporation is the vaporization enthalpy of water.
- Bound water: Water is physically adsorbed on the solid phase. The water activity a_{w} is less than 1 and is given by the desorption isotherms characteristic of the hygroscopic equilibrium. The required energy to pull bound water out the solid is called desorption heat. This energy is higher when the water molecule is closer to the solid wall.

As bound water evaporation requires more energy (the sum of vaporization and desorption enthalpy), its elimination is posterior to the free water one. When all the free water has disappeared, the material is said to be in the hygroscopic field. The two-phase hypothesis of the model imposes that moisture (free water as well as bound water) always fills completely the free spaces within the solid.

First of all, let us specify that it is considered that the convective transport of the moisture resulting from the pressure gradient of the liquid phase is created and controlled by the capillary pressure evolution at the surface of the two-phase medium.[27,28] Indeed, the contact between the air, the solid, and the liquid phase at the surface of the gel imposes necessarily the appearance of a meniscus associated to the capillary pressure P_{C} (Figure 2) usually defined by:

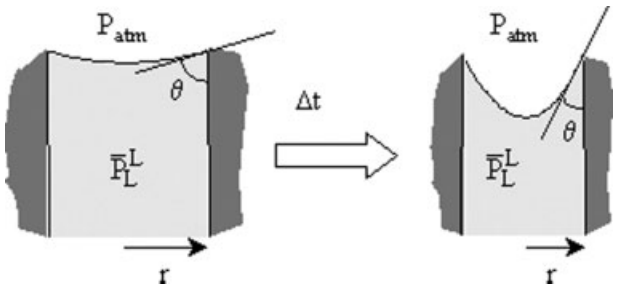

Figure 2. Capillary pressure and evolution due to shrinkage.

$$P_C = \frac{2\tau \cos\theta}{r}, \tag{44}$$

where τ, θ, and r represent the surface tension of the fluid, the wetting angle, and the pore radius, if one assumes a porous structure for the gel.

Both the actions of the evaporation (wetting angle decrease) and of the shrinkage (pore radius diminution) lead, in accordance with Eq. 44, to a capillary pressure increase. Under the hypothesis, very reasonable for a low and medium temperature convective drying, that the air pressure keeps constant and equal to the atmospheric pressure P_{atm}, the capillary pressure growth imposes a diminution of the liquid phase pressure according to the relation

$$\bar{P}_L^L = P_{atm} - P_C. \tag{45}$$

The pressure gradient resulting from the diminution of $\bar{P}_L^L$ at the surface is then responsible for the liquid phase movement.

Classically, the convective drying of a hygroscopic material shows four different steps.

- A very short transient period compared to the whole drying process, corresponds to the heating of the product to the wet bulb temperature T_h, characteristic of the drying air.
- A constant evaporation rate phase, often isenthalpic, which is similar to the evaporation of a liquid water film. During this period the temperature remains constant and is equal to the wet bulb temperature T_h. This phase carries on so long as the surface is supplied with free moisture from inside the material. The heat flux exchanged by convection between the air and the product is entirely used to evaporate water.
- A first slowing down period begins when the material surface reaches the hygroscopic field boundary water content (W_{hygr}). Then, a part of the product is in the hygroscopic field within which there is bound water migration.
- A second slowing down phase appears when the whole material is in the hygroscopic field. At this time, only bound water is eliminated. The evaporation rate decreases more quickly than in the former period. This period ends when the material reaches the equilibrium moisture content W_{eq}, which depends on drying conditions.

From now on, even before performing simulations, some reserves can already be advanced on the representation of the slowing down phases at the end of drying because of the model hypothesis.

- First, the two-phase hypothesis prevents from taking into account the creation of porosity and the appearance of a vapor phase which can occur when the solid phase definitively locks mechanically.
- Second, in this model, the convective transport of moisture results from the pressure gradient of the liquid phase created by the capillary pressure evolution at the surface of the two-phase medium. This mechanism, physically true for free water, becomes a hazardous extrapolation for bound water as the capillary pressure is not well defined for the weak moisture contents. The transport process of bound water is undoubtedly different but the way to describe it at the scale of continuum mechanics has not been exanimate during this work.
  Obviously, the classical approach in literature which consists in linking the convective transport of moisture (free water as well as bound water) to the water content gradient using a nonphysical law enables to avoid these problems at the end of drying. Nevertheless, for the reasons already developed in this manuscript, this phenomenological approach is still rejected.

Now, in order to apply the model to the drying of a gelatin gel and to perform the simulations, the initial and boundary conditions as well as the physical properties of the product have to be defined.

Initial conditions

Initials fields of liquid pressure, liquid volume fraction and temperature in the medium are uniform:

$$t = 0, \forall x_3 \qquad \bar{P}_L^L = \bar{P}_L^{L0}, \tag{46}$$

$$t = 0, \forall x_3 \qquad \varepsilon_L = \varepsilon_L^0, \tag{47}$$

$$t = 0, \forall x_3 \qquad \bar{T} = \bar{T}^0. \tag{48}$$

Boundary conditions

As previously stated, boundary conditions are obtained by using the boundary layer theory and the classical heat and mass transfer analogy in order to express the fluxes.

$$\left(\bar{\rho}_S \bar{h}_S^S \left(\bar{\mathbf{v}}_S^S - \mathbf{w}_{surf}\right) + \bar{\rho}_L \bar{h}_L^L \left(\bar{\mathbf{v}}_L^L - \mathbf{w}_{surf}\right) - \underline{\underline{\lambda}}_{eff} \cdot \nabla \bar{T}\right) \cdot \mathbf{n} = h_T(\bar{T}_{surf} - T_\infty) + h_m(\rho_{vsurf} - \rho_{v\infty}) h_{vsurf}, \tag{49}$$

$$\bar{\rho}_L \left(\bar{\mathbf{v}}_L^L - \mathbf{w}_{surf}\right) \cdot \mathbf{n} = h_m(\rho_{vsurf} - \rho_{v\infty}). \tag{50}$$

Here h_{vsurf} is the enthalpy of the vapor evaluated at the surface temperature $\bar{T}_{surf}$,

$$h_{vsurf} = Cp_v(\bar{T}_{surf} - T_{ref}) + \Delta H_v^{ref}, \tag{51}$$

and ρ_{vsurf} is the mass concentration of vapor at the surface of the two-phase medium, more precisely the concentration at the interface between the liquid phase and the ambient air. This concentration is given by assuming that the ambient air is a perfect mixture of ideal gas:

$$\rho_{vsurf} = M_v P_{vsurf} / R\bar{T}_{surf}$$

The vapor pressure at the surface is calculated from the water activity under the classical assumption of the thermodynamical equilibrium

Table 1. Physical Parameters of the Two-Phase Medium

$\bar{\rho}_s^s$	Density of the solid phase (kgm^{-3})	1341
K	Permeability (m^2)	$10^{-11} \cdot \varepsilon_L^3$
C_{pS}	Heat capacity of the solid phase ($Jkg^{-1}K^{-1}$)	1804
C_{pL}	Heat capacity of the liquid phase ($Jkg^{-1}K^{-1}$)	4182
λ_{eff}	Thermal conductivity of the two-phase medium ($Wm^{-1}K^{-1}$)	$\lambda_{eff} = \varepsilon_L\lambda_L + \varepsilon_S\lambda_S$ $\lambda_L = 0.6071$ $\lambda_S = 0.3334$
W_{hygr}	Moisture content limit between free and bound water	0.3
a_w	Water activity	1 if $W > W_{hygr}$ else $W^* = \frac{a_w A}{(1-Ba_w)(1+Ca_w)}$
$\Delta\bar{H}_D^L$	Desorption enthalpy (Jkg^{-1})	0 if $W > W_{hygr}$ else $\exp(7.0078 - 93.5125W^{2.5}) \times 10^3$
Rheology	Lamé coefficients	$\lambda = -9.92 \times 10^8 + 8.58\times10^9 \exp(-\varepsilon_L)$ $\mu = \exp(21.82 - 11.91\varepsilon_L^{1.5})$

*$A = -0.0002\,\bar{T}^2 - 0.0142\,\bar{T} + 2.9099$, $B = 0.0022\,\bar{T} + 0.7226$, $C = -0.0028\,\bar{T}^2 + 0.0327\,\bar{T} + 22.629$.

$$P_{vsurf} = a_w P_{vsat\ surf},$$

where $P_{vsat\ surf}$ is the saturation vapor pressure evaluated at $\bar{T}_{surf}$. The vector $\mathbf{w}_{surf}$ is the velocity of the interface between the two-phase medium and the external fluid. This velocity can be easily evaluated by noting that the surface of the gel sample considered here is not permeable to the solid:

$$\bar{\rho}_S\left(\bar{\mathbf{v}}_S^S - \mathbf{w}_{surf}\right) \cdot \mathbf{n} = 0. \tag{52}$$

From Eq. 52, it ensues immediately that

$$\bar{\mathbf{v}}_S^S \cdot \mathbf{n} = \mathbf{w}_{surf} \cdot \mathbf{n}. \tag{53}$$

Hence, Eqs. 49 and 50 can finally be written as follows:

$$\left(\bar{\rho}_L\bar{h}_L^L\left(\bar{\mathbf{v}}_L^L - \bar{\mathbf{v}}_S^S\right) - \underline{\underline{\lambda}}_{eff} \cdot \nabla\bar{T}\right) \cdot \mathbf{n} = h_T(\bar{T}_{surf} - T_\infty) + h_m(\rho_{vsurf} - \rho_{v\infty})h_{vsurf}, \tag{54}$$

$$\bar{\rho}_L\left(\bar{\mathbf{v}}_L^L - \bar{\mathbf{v}}_S^S\right) \cdot \mathbf{n} = h_m(\rho_{vsurf} - \rho_{v\infty}). \tag{55}$$

The last condition available is associated to the total momentum conservation 29. By neglecting the effects of the ambient pressure, the stress continuity at the interface allows the equation

$$\underline{\underline{\boldsymbol{\sigma}}} \cdot \mathbf{n} = \mathbf{0}. \tag{56}$$

It must be stressed that only one condition related to momentum conservation is written although there were two original momentum conservation equations, one for each phase. It means one boundary condition misses undoubtedly. According to the phenomenology previously described, one can imagine that the missing relation could be provided by the experimental knowledge of the capillary pressure at the interface between the diphasic medium and the ambient air. At the surface, we would have:

$$\bar{P}_L^L = P_{atm} - P_C(\varepsilon_L) \tag{57}$$

Equation 57 should ensure a unique solution $\bar{P}_L^L$ for the Eq. 43. However, any data concerning capillary pressure and how to measure it in our case can be found in literature. Then, because only the gradient has an influence on the other unknowns of the problem, we decide to solve the Eq. 43 without the condition 57 by using a method that preserves the gradient. This technique, called singular value decomposition method,[29] is not detailed here.

Physical properties of the gelatin gel

Physical parameters[15,17] of the two-phase medium are given in the Table 1.

Before presenting our results, we would like to focus on three points.

- Because of the absence of information on permeability, an expression (Table 1) that imposes a decrease with the volume fraction of liquid has been chosen to carry out simulations. This parameter seems to be difficult to measure experimentally for a deformable medium. Consequently, this determination constitutes a practical perspective of this work using the numerical code by inverse method.
- The one-dimensional configuration which is considered leads us to reduce the elastic behavior to an ideal shrinkage. We suppose that the material do not build up stresses during the process, and then, the volumetric shrinkage is the real shrinkage. We have

$$\underline{\underline{\boldsymbol{\varepsilon}}} = \underline{\underline{\boldsymbol{\varepsilon}}}^v \tag{58}$$

Calculation of the load induced by the volume change due to solvent removal is based on the following spherical volumetric strain tensor

$$\underline{\underline{\boldsymbol{\varepsilon}}}^v = \varepsilon^v\underline{\underline{\mathbf{I}}} \text{ with } \varepsilon^v = \frac{1}{3}\frac{\Delta\varepsilon_L}{1-\varepsilon_L} \tag{59}$$

In this relation, $\Delta\varepsilon_L$ represents the variation of the liquid fraction between the current and the previous time step of the time discretization.

- As previously mentioned, the thermal conductivity of the two-phase medium should be measured experimentally in function of the water content. As we do not have these data at our disposal, we use the simple expression given in Table 1.

Simulation results and analysis

Simulations are carried out with a constant time step (δt = 0.1 s) in 1D configuration following the sample thickness

Table 2. Drying Air Characteristics Selected for the Two Simulations

	Drying Air Characteristics		
	T_∞ (°C)	RH_∞ (%)	h_T ($Wm^{-2}K^{-1}$)
Condition 1	35	55	10
Condition 2	75	20	15

(e = 0.01 m). This thickness is discretized by 51 nodes regularly spaced at t = 0. Two drying conditions are simulated with the numerical code (Table 2): a soft one (condition 1) and a hard one (condition 2). In the numerical code, h_T is imposed rather than being calculated from the air velocity.

Profiles and kinetics of liquid phase pressure $\bar{P}_L^L$, of water content W and of temperature $\bar{T}$ for the two drying conditions given in Table 2, are presented in Figures 3 and 4. The water content W is deduced from the liquid volume fraction as follows:

$$W = \frac{\varepsilon_L \bar{\rho}_L^L}{(1-\varepsilon_L)\bar{\rho}_S^S}$$

For the kinetics, the evolutions of these variables are given at the surface $[x_3 = e(t)]$ and at the center $[x_3 = e(t)/2]$ of the medium. Moreover, the shrinkage velocities of the two-phase medium are equally plotted during the whole simulation (Figure 5). Nevertheless, for a clearer representation, these velocity profiles are only shown for the $[e(t)/2, e(t)]$ field.

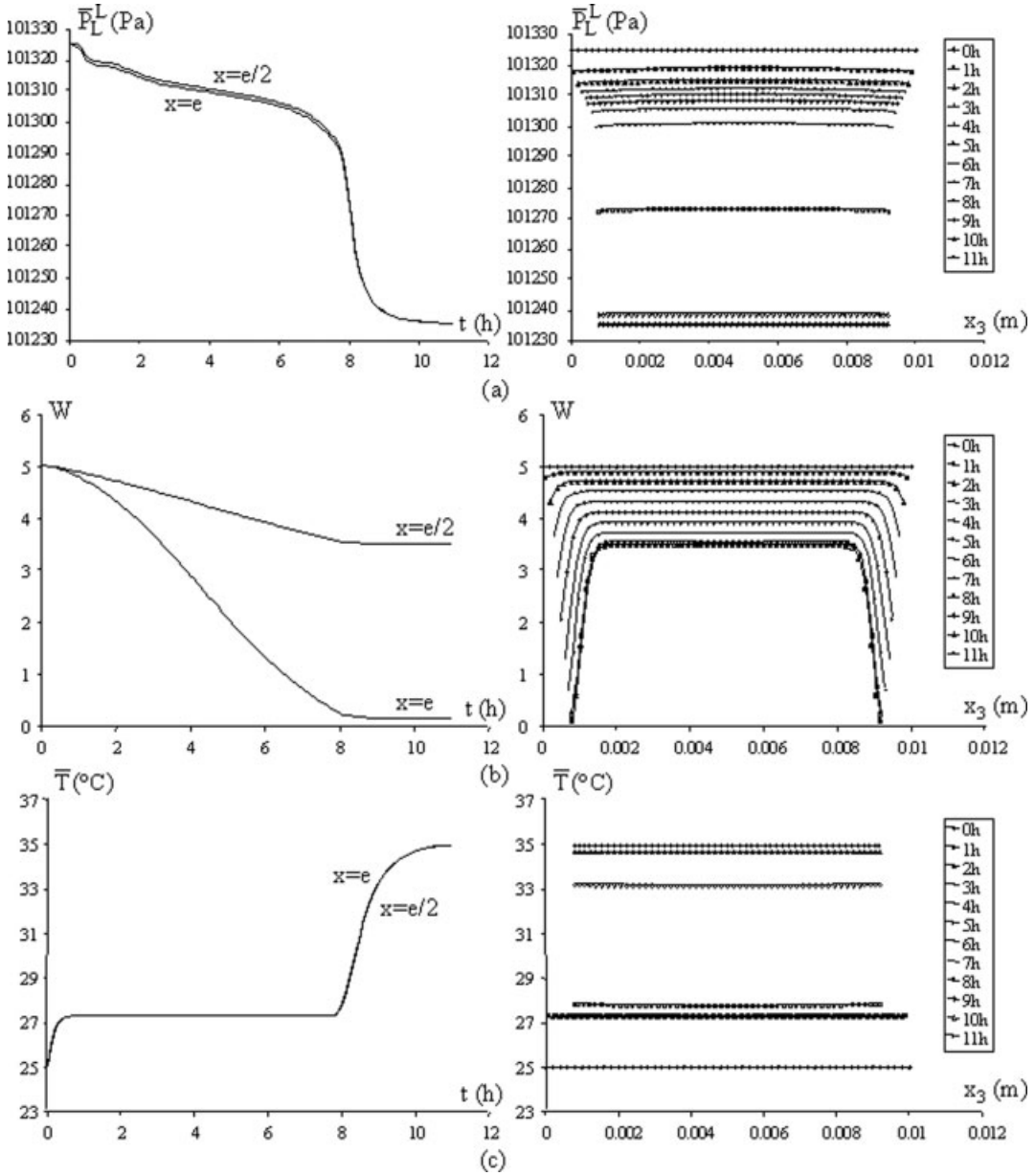

Figure 3. Kinetics and profiles of the liquid phase pressure (a), of the moisture content (b), and of the temperature (c) for the simulation condition 1 (Table 2).

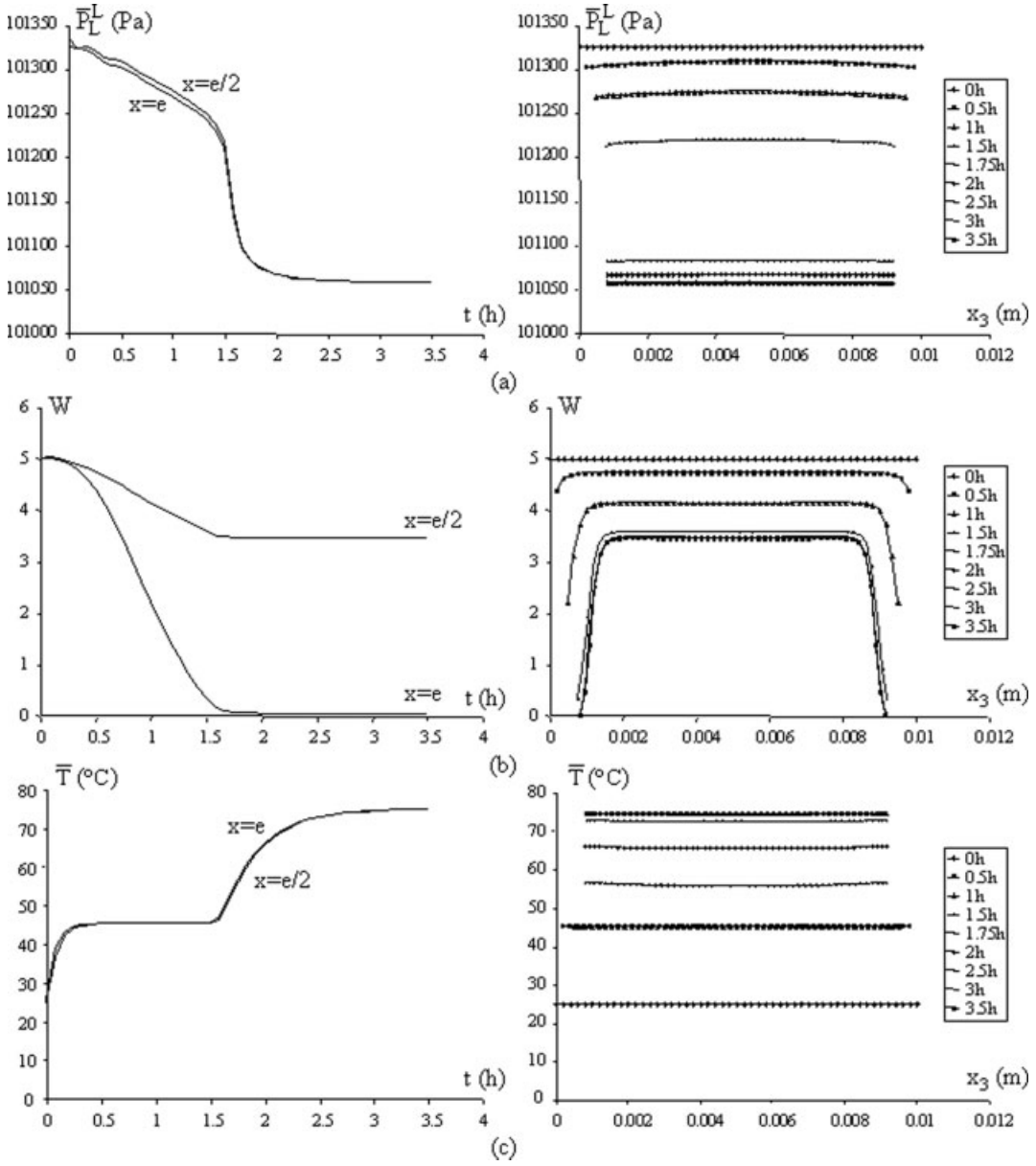

Figure 4. Kinetics and profiles of the liquid phase pressure (a), of the moisture content (b), and of the temperature (c) for the simulation condition 2 (Table 2).

The simulated process follows the drying kinetic given in the Figure 6.

The physical phenomenon analysis, from the simulation results and consequently from the mathematical model, is carried out for each of the observed drying phases (points A, B, and C in the Figure 6). These points A, B, and C correspond respectively to the simulation times 5 min, 4 h, and 8 h for the condition 1. The analysis is also valid for the condition 2.

Transient Period (Point A). The appearance of the liquid phase pressure gradient is shown in the Figure 7. It can be observed equally in the pressure kinetics (Figures 3a and 4a), in which a divergence between the values at the surface and at the center of the material is visible. This gradient, very small at the beginning, increases as the medium temperature gets closer to the wet bulb one.

The comparison of the pressure and the water content profiles given in the Figure 8 underlines the sensible difference between the gradients of these two variables. Contrary to the literature assertions any link can be observed between the moisture content gradient and the convective transport of the liquid phase. For instance, the movement of the liquid phase at the center of the material ($\nabla \bar{P}_L^L \neq 0$) would not exist if the moisture content gradient was the driving term ($\nabla W = 0$). This comment can be spread to the whole process (Figures 9 and 10).

As only a part of the heat supplied by the drying air is used to evaporate water, the material is heated until its temperature reaches the wet bulb temperature value (27.2°C for the condition 1 and 45°C for the condition 2, (Figures 3c and 4c)).

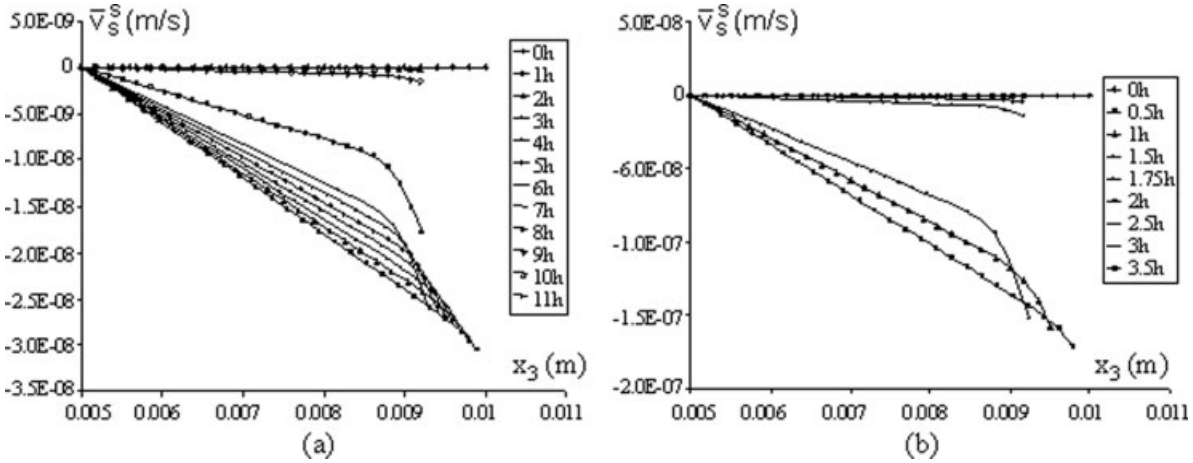

Figure 5. Profile of the solid phase velocity for the condition 1 (a) and the condition 2 (b) (Table 2).

Constant Evaporation Rate Phase (Point B). Once the wet bulb temperature value is reached, the temperature stabilizes uniformly within the material (Figures 3c and 4c). The whole heat supplied by the air is consumed by the water evaporation at the surface with a constant rate (Figure 6).

Pressure gradients (Figures 3a and 4a) drive the convective transport of the free water towards the surface (Figure 9). As a consequence to this movement, the solid matrix gets out of shape and shrinks in the opposite direction (Figure 5) to fill the free spaces liberated by the liquid phase. In accordance with the great departure of water near the surface, the solid phase velocity shows a stronger increase in this area (Figure 5).

As previously explained, during drying progress, the liquid pressure profile is moving to lower values because of the capillary pressure augmentation. As the liquid phase pressure near the surface is reduced, the values of the whole field of pressure within the material also decrease because the gradient keeps constant, in coherence with the constant evaporation rate at the surface. In spite of the liquid pressure profile displacement towards lower values, the pressure gradient within the sample keeps sensitively the same level. This is illustrated in kinetics 3a and 4a, by the same divergence held between the liquid phase pressure at $x_3 = e(t)$ and $x_3 = e(t)/2$ during this phase. This gradient, depending on drying conditions, results in a greater transport of the free moisture in the condition 2. Consequently, this is the condition for which the sample reaches the hygroscopic field the earlier ($W_{hygr} = 0.3$).

First Slowing Down Period (Point C). This phase begins as soon as the surface enters the hygroscopic field. The decrease of the evaporation rate due to the reduction of the water activity involves an excess of heat which gives rise to an augmentation of the surface temperature. By conduction, the heat flux reaches quickly the center of the material. The temperature increases to the value of the air one which points out the end of drying (Figures 3c and 4c).

Let us remind that in the model, the hygroscopic behavior of the material is taken into account only through the change of the water enthalpy due to the appearance of the desorption enthalpy within the material and through the reduction of the water activity following the desorption isotherms at the surface. The diminution of the water activity is responsible for the evaporation rate decrease.

As previously explained in this manuscript, contrary to free moisture, the movement of bound water is certainly not caused by the gradient of the liquid phase pressure induced by the capillary pressure evolution. As a consequence, the phenomenon analysis during this slowing down period is limited to the verification of the coherence between the simulated results and the mathematical model.

The main observation consists in an augmentation of the pressure gradient at the surface despite the flux diminution (Figures 3a, 4a, and 10). This variation is due to a quick decrease of the permeability with the liquid volume fraction given by the relation (Table 1):

$$K = 10^{-11} \cdot \varepsilon_L^3 \tag{60}$$

The drying of the surface is then shown by a faster diminution of the pressure profile during this last phase (Figures 3a and 4a).

The surface moisture content reaches its equilibrium value, given by the desorption isotherms, and keeps constant. Con-

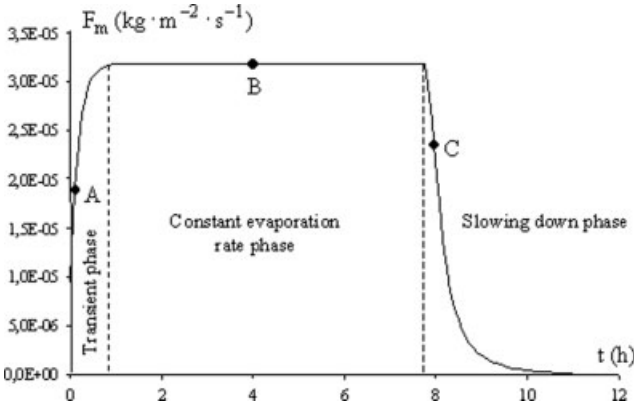

Figure 6. Drying kinetic for the simulation condition 1 (Table 2).

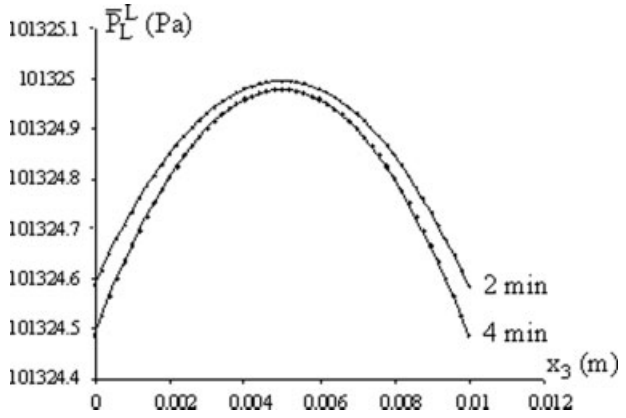

Figure 7. Liquid phase pressure profile at t = 2 min and t = 4 min for the simulation condition 1 (Table 2).

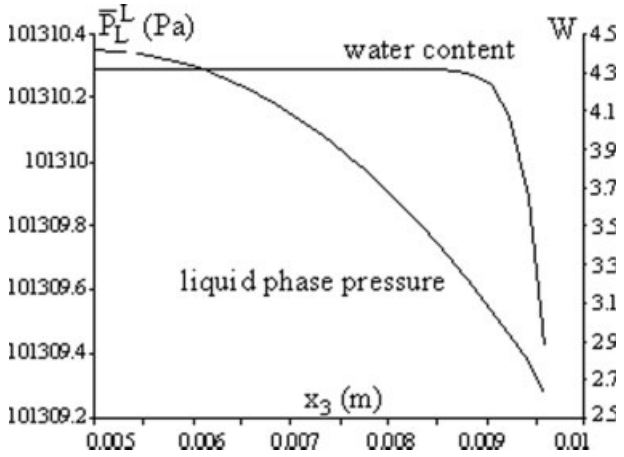

Figure 9. Liquid phase pressure and moisture content profiles at t = 4 h for the simulation condition 1 (point B in Figure 6).

sequently, at the surface, the liquid volume fraction is also constant and as indicated by the Eq. 60 the permeability does not vary anymore. The evaporation rate reduction then imposes a pressure gradient decrease at the surface. The liquid pressure stabilizes around the values of 101,235 Pa for the condition 1 and 101,058 Pa for the condition 2 with quasi-flat profiles (only an exaggeration of the scale enables to see the bends).

Once the liquid pressure is constant and uniform within the sample, the driving term of the convective transport, that is to say the liquid phase pressure gradient, disappears. Consequently the material does not dry any more; its water content stabilizes but with a nonflat profile. Drying seems to be finished whereas the material heart is far from entering the hygroscopic field. This analysis explains the absence of the second slowing down period observed in the drying kinetics and illustrated in the Figure 6 for the condition 1.

These results, even if they are logically coherent with the physical mechanisms scheduled by the model, are not completely satisfying. Indeed, on one hand, the final moisture content is very high within the material and on the other hand, it is usual experimentally to finish the process with flat profiles. Even if the limits of the model at the end of drying, already underlined, such as the absence of a rigorous description of the bound water transport or the impossibility of the appearance of a vapor phase, constitute a probable explanation, experimental tries are performed with the aim to compare the results to the simulated one.

Confrontation to Experiments. As only moisture content profiles show a nontypical behavior, analysis are concentrated on this parameter, without taking care of temperature repartition. It is reminded that these experiments are not carried out in order to validate quantitatively the model, but to provide some confidence in a physical description without fitted parameter. Indeed, for the simulations, some physical properties of the gel such as the permeability have been imposed arbitrarily. The selected drying condition (T_∞ = 35°C, RH_∞ = 55%, and V_∞ = 1 m s^{-1}) corresponds to the simulated condition 1.

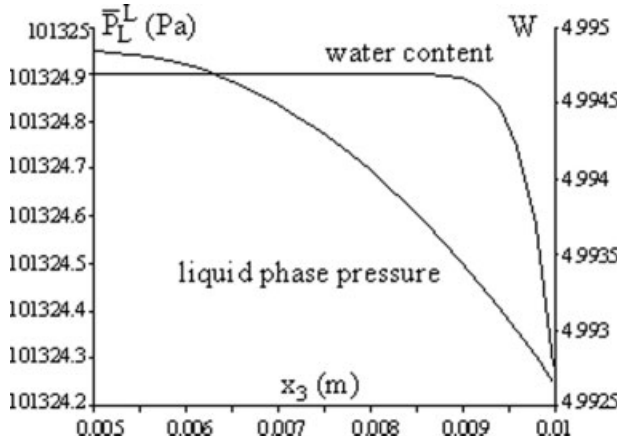

Figure 8. Liquid phase pressure and moisture content profiles at t = 5 min for the simulation condition 1 (point A in Figure 6).

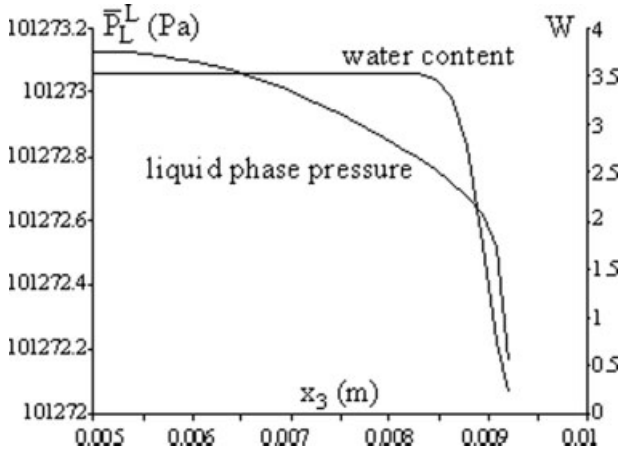

Figure 10. Liquid phase pressure and moisture content profiles at t = 8 h for the simulation condition 1 (point C in Figure 6).

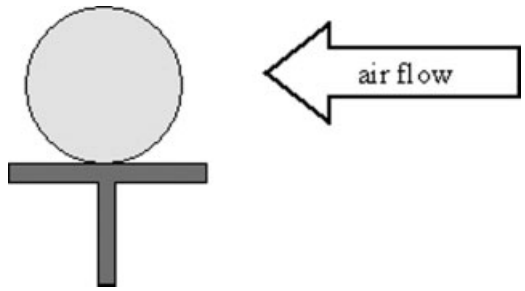

Figure 11. Situation of the sample in the drying tunnel.

Gelatin samples are obtained by a sol–gel transition process. The gelatin is mixed with water to be hydrated during 25 min. Then the mixture is maintained at a constant temperature of 55°C during 30 min which leads to a colloidal solution. This solution is injected in a mould where it is cooled to obtain a 0.015 m thickness and 0.038 m diameter gel sample. The one-dimension drying is imposed by isolating the lateral surfaces with paste. The sample is then pasted vertically on a stand in the drying tunnel as shown in Figure 11.

The water contents profiles are determined by slicing the sample after different times of drying (Figure 12). As this method is destructive, each profile corresponds to one manipulation. This method which is the simplest to carry into effect is not more accurate for at least two reasons:

- It supposes a perfect reproducibility between two successive tries,
- Moisture can be lost during slicing.

Nevertheless, as our objective is just a qualitative validation as previously mentioned, this method is sufficient. For a quantitative validation, nondestructive techniques, such γ-rays, NMR, etc., will have to be privileged.

Each slice is then heated to 100°C in an oven during 24 h to determine its dry weight and to deduce its moisture content. Figure 13 shows the obtained results and compares them with the corresponding simulated one.

At the beginning of drying (until $t = 5$ h) the experimental and simulated profiles show similar appearances (Figure 13). The moisture is essentially eliminated near the surface. Consequently, the water content gradients appear only near the surface and do not exist within the material. The choice of this work to treat the water convective movement with its natural driving term, that is to say the liquid phase pressure gradient is reinforced by the qualitative agreement between the calculated and experimental curves.

It is impossible to determine the moisture content profiles after 30 h of drying. Indeed, samples become rigid and very

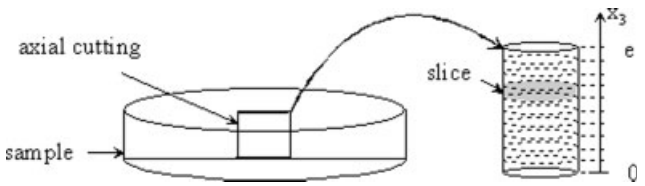

Figure 12. Slicing of the sample.

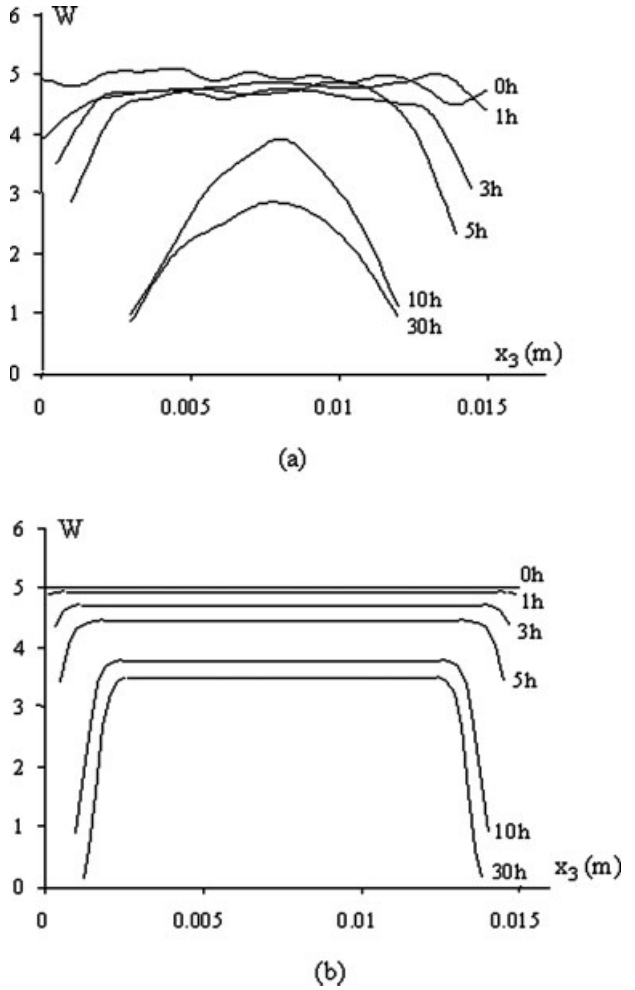

Figure 13. Experimental (a) and simulated (b) moisture content profiles.

hard, essentially at the surface, preventing from slicing. Nevertheless, after 70 h of drying, the average water content of a sample has been measured to 0.25, a value greatly lower than the one reached within the material during simulations. The limits of our model at the end of drying previously mentioned can explain these divergences. Firstly, it does not take into account the creation of porosity at the surface with the appearance of a vapor phase and the flow through this porous bed. A perspective to this work consists in joining this model to a three phase one used for classical porous media.[30] Secondly, the treatment of the convective transport as resulting from the liquid phase pressure gradient is not adapted to bound water.

Conclusion

The model solved in this work allows describing the heat and mass transports during drying of deformable media considered as an immiscible two-phase system. A continuum approach based on volume averaging theory is adopted. The main novelty is that although a global stress strain relation for the homogenized medium is used, no arbitrary link

between liquid pressure and liquid volume fraction leading to an equivalent transport coefficient is introduced. Indeed, as this coefficient must be identified numerically by matching experimental and predicted data, it is unjustly linked to the experimental set-up because of the approximations in the description of the boundary conditions. Here, as for the liquid phase, both volume and mass conservation equations are kept for the solid phase. These two independent equations, rather than one of the two as it is commonly the case in literature, enable the unknown liquid pressure to be calculated rigorously.

Low or middle temperature convective drying of gelatin is the example chosen in order to illustrate the capacity of the model. Only one-dimensional configuration is considered in such a way that the elastic behavior is reduced to an ideal shrinkage. However, the numerical results and the qualitative comparison to experimental data provide some confidence in the proposed model and motivate undoubtedly a two-dimensional resolution that will allow taking into account the rheological behavior.

Notation

A_{SL} = area of solid-liquid phases interface within the averaging volume, m^2
a_w = water activity
cst = constant value
C_p = constant pressure heat capacity, J kg^{-1} K^{-1}
e = thickness of the sample, m
h_α = enthalpy per unit mass of the α-phase, J kg^{-1}
h_m = mass transfer coefficient, m s^{-1}
h_T = heat transfer coefficient, W m^{-2} K^{-1}
h_{vsuf} = enthalpy per unit mass of the vapor at the surface of the two phase medium, J kg^{-1}
$\underline{\underline{\mathbf{D}}}$ = equivalent transport tensor, m^2 s^{-1}
$\underline{\underline{I}}$ = tensor identity
$\underline{\underline{\mathbf{K}}}$ = permeabilities tensor, m^2
$\overline{M_v}$ = molar mass of the vapor, kg mol^{-1}
$\boldsymbol{n}$ = outward unit normal vector, m
$\boldsymbol{n}_{\alpha\beta}$ = unit normal vector pointing from the α-phase toward the β-phase, m
P_{atm} = atmospheric pressure, Pa
P_C = capillary pressure at the surface of the two phase medium, Pa
P_L = pressure of the liquid phase, Pa
$P_{vsat\ surf}$ = saturation vapor pressure at the surface of the two phase medium, Pa
r = pore radius, m
R = ideal gas constant, J mol^{-1} K^{-1}
RH_∞ = relative humidity of the ambient air, %
t = time (s)
T = temperature of the medium, K
T_h = wet bulb temperature of the ambient air, K
T_{ref} = reference temperature for the enthalpy, K
T_{surf} = temperature at the surface of the two phase medium, K
T_α = temperature of the α-phase, K
T_∞ = temperature of the ambient air, K
$\boldsymbol{u}$ = displacement vector, m
$\boldsymbol{v}_\alpha$ = velocity vector of the α-phase, m s^{-1}
$\boldsymbol{v}_\infty$ = velocity vector of the ambient air, m s^{-1}
V = averaging volume, m^3
V_α = volume of the α-phase within the averaging volume, m^3
$\boldsymbol{w}$ = velocity vector of the internal solid-liquid interface, m s^{-1}
$\boldsymbol{w}_{surf}$ = velocity vector of the two phase medium-ambient air interface, m s^{-1}
W = moisture content dry basis
W_{hygr} = maximum bound moisture content dry basis (limit of the non hygroscopic region)
W_{surf} = moisture content dry basis at the surface of the two phase medium
W_{eq} = equilibrium moisture content dry basis
x_3 = 1D coordinate following the thickness, m
δt = time step for the numerical resolution, s
ΔH_v^{ref} = latent heat of vaporization at T_{ref}, J kg^{-1}
$\Delta \bar{H}_D^L$ = Desorption enthalpy, J kg^{-1}
∇ = gradient operator
$\nabla\cdot$ = divergence operator
ε_α = volume fraction of the α-phase
$\underline{\underline{\boldsymbol{\varepsilon}}}$ = total strain tensor
$\underline{\underline{\boldsymbol{\varepsilon}}}^{\overline{v}}$ = volumetric strain tensor
$\underline{\underline{\boldsymbol{\varepsilon}}}^{*}$ = elastic strain tensor
λ = first Lamé's coefficient, Pa
λ_α = thermal conductivity of the α-phase,W m^{-1} K^{-1}
$\underline{\underline{\boldsymbol{\lambda}}}_{eff}$ = effective thermal conductivity tensor, W m^{-1} K^{-1}
μ = second Lamé's coefficient, Pa
μ_L = stress viscosity coefficient of the liquid phase, Pa s
ν_L = kinematic viscosity of the liquid phase, m^2 s^{-1}
θ = wetting angle, °
ρ_α = mass density of the α-phase, kg m^{-3}
ρ_{vsurf} = mass concentration of vapor at the surface of the two-phase medium, kg m^{-3}
$\underline{\underline{\boldsymbol{\sigma}}}$ = total stress tensor, Pa
$\underline{\underline{\boldsymbol{\sigma}}}_\alpha$ = stress tensor of the α-phase, Pa
τ = surface tension of liquid, N m^{-1}
$\bar{\Psi}$ = phase average of quantity Ψ
$\bar{\Psi}^\alpha$ = intrinsic phase average of quantity Ψ
$\tilde{\Psi}$ = deviation of a quantity Ψ

Literature Cited

1. Hasatani M, Itaya Y. Drying induced strain and stress: a review. *Drying Technol*. 1996;14:1011–1040.
2. Katekawa ME, Silva MA. A review of drying models including shrinkage effects. *Drying Technol*. 2006;24:5–20.
3. Biot MA. Theory of elasticity and consolidation for a porous anisotropic solid. *J Appl Phys*. 1955;26:182–185.
4. Dormieux L, Barboux P, Coussy O, Dangla P. A macroscopic model of the swelling phenomenon of a saturated clay. *Eur J Mech A Solids*. 1995;14:981–1004.
5. Coussy O, Dormieux L, Detournay E. From mixture theory to Biot's approach for porous media. *Int J Solids Struct*. 1998;35:4619–4635.
6. Couture F, Roques MA, Bogdanis E. Towards thermo-hydro-rheology. Proceeding of the Second Inter-American Drying Conference (IADC), Veracruz, Mexique, 08-10/07 (Walizewski KN, editor). Veracruz, Mexico: I.T.V. 2001:91–105.
7. Jomaa W, Puiggali JR. Drying of shrinking materials: modelling with shrinkage velocity. *Drying Technol*. 1991;9:1271–1293.
8. Kechaou N, Roques MA. A variable diffusivity model for drying of highly deformable materials. In: Mujumdar AS, Roques M, editors. *Drying'89*. New York: Hemisphere, 1989:332–338.
9. Ketelaars AAJ, Jomaa W, Puiggali JR, Coumans WJ. Drying shrinkage and stress. *Drying'92*, International Drying Symposium, 1992, Part A:293–303.
10. Mercier F, Puiggali JR, Roques MA, Brunard N, Kolenda F. Convective and micro-wave drying of alumina beads. In: Modelling of shrinkage. 3rd World Congress on Particle Technology, 06-09/07, Brighton, UK. 1998.
11. Mrani I, Bénet JC, Fras G. Transport of water in a biconstituent elastic medium. *Appl Mech Rev*. 1995;48:717–721.
12. Sfair AL, Couture F, Laurent S, Roques M. Modeling of heat and mass transport in two-phase media by considering liquid pressure. *Drying Technol*. 2004;22:81–90.
13. Whitaker S. Flow in porous media III: deformable media. *Transport Porous Media*. 1986;1:127–154.
14. Sfair AL. Modélisation des phénomènes de transport en milieu déformable diphasique: prise en compte de la pression liquide. PhD Thesis, University of Pau. 2004.
15. Cornillon P. Mesure et modélisation des différents types d'eau et des propriétés thermophysiques des gels alimentaires congelés. PhD Thesis, University Claude Bernard Lyon I. 1992.

16. Djabourov M, Lechaire JP, Gaill F. Structure and rheology of gelatin and collagen gels. *Biorheology*. 1993;30:191–205.
17. Zagrouba F. Séchage mixte par convection et un apport rayonnant micro-onde des milieux déformables. Modélisation des phénomènes de transferts de chaleur et de matière. PhD Thesis, Ecole Nationale Supérieure des Industries Chimiques. 1993.
18. Ross-Murphy SB. Structure and rheology of gelatin gels. *Imaging Sci J*. 1997;45:205–209.
19. Marle CM. Ecoulements monophasiques en milieu poreux. *Rev Inst Fr Petrole*. 1967;22:1471–1509.
20. Slattery JC. *Momentum, Energy and Mass Transfer in Continua*. New York: Robert E. Krieger, 1981.
21. Whitaker S. Simultaneous heat, mass and momentum transfer in porous media: a theory of drying. In: Irvine TF, Hartnett JP, editors. *Advances in Heat Transfer*, *Vol* 13. New York: Academic Press, 1977a;119–203.
22. Whitaker S. *Fundamental Principles of Heat Transfer*. New York: Pergamon, 1977b.
23. Whitaker S. *The Method of Volume Averaging*. Netherlands: Kluwer Academic, 1999.
24. Quintard M, Whitaker S. One- and two-equation models for transient diffusion processes in two-phase system. In: Irvine TF, Hartnett JP, editors. *Advances in Heat Transfer*, *Vol* 23. New York: Academic Press, 1993:369–464.
25. Chausi B, Couture F, Roques M. Modelling of multicomponent mass transport in deformable media, application to dewatering impregnation soaking process. *Drying Technol*. 2001a;15:423–432.
26. Chausi B, Couture F, Roques MA. Modelling of mass transfer during dewatering-impregnation-soaking. Proceeding of the Second Inter-American Drying Conference (IADC), Veracruz, Mexique, 08-10/07 (Walizewski KN, editor). Veracruz, Mexico: I.T.V. 2001b: 526–534.
27. Brinker CJ, Scherer GW. *Sol-Gel Science: The Physics and Chemistry of Sol-Gel Processing*. New York: Academic Press, 1990.
28. Bernada P. Analyse expérimentale et modélisation de la migration de liants dans une couche papetière soumise à un flux de séchage. PhD Thesis, Ecole Nationale Supérieure d'Arts et Métiers—Centre de Bordeaux. 1995.
29. Press WH, Flannery BP, Teukolsky SA. *Numerical Recipes in Fortran: The Art of Scientific Computing*, *2nd ed*. Cambridge: Cambridge University Press, 1992.
30. Couture F. Modélisation fine d'un problème de séchage: développement d'outils adaptés. PhD Thesis, University Bordeaux I. 1995.

Manuscript received Oct. 26, 2006, and revision received Apr. 5, 2007.